An Aerodynamic Optimization Method Based on the Inverse Problem Adjoint Equations

A. Iollo, M. Ferlauto, and L. Zannetti

Dipartimento di Ingegneria Aeronautica e Spaziale Politecnico di Torino, C.so Duca degli Abruzzi 24, 10129 Torino, Italy
E-mail: iollo@aethon.polito.it, ferlauto@athena.polito.it, zannetti@polito.it

An adjoint optimization method, based on the solution of an inverse flow problem, is proposed. Given a certain performance functional, it is necessary to find its extremum with respect to a flow variable distribution on the domain boundary, for example, pressure. The adjoint formulation delivers the functional gradient with respect to such a flow variable distribution, and a descent method can be used for optimization. The flow constraints are easily imposed in the parameterization of the distributed control, and therefore those problems with several strict constraints on the flow solution can be solved very efficiently. Conversely, the geometric constraints are imposed either by additional partial differential equations, or by penalization. By adequately constraining the geometric solution, the classical limitations of the inverse problem design can be overcome. Several examples pertaining to internal flows are given. © 2001 Academic Press

Key Words: adjoint method; inverse problem; optimization; compressible flow.

1. INTRODUCTION

Aerodynamic design can be assisted in two essentially different ways. One, the classic approach, is based on the inverse problem solution; the other, which is more recent, relies on numerical optimization.

In the inverse problem one must usually determine unknowns that are given in the natural, i.e., direct position of the problem. For example, a typical inverse problem is to find the airfoil geometry, given the flight speed and the pressure distribution on its surface. In the classical works of Mangler [1] and Lighthill [2] the airfoil inverse problem was solved in the framework of potential flows and with the use of conformal mapping. Further developments of this solution method are extensively accounted in [3] and are related to the introduction of viscous models for laminar and turbulent flows and to the solvability conditions of the problem. Other examples of inverse problem solution methods are

87

found in the collection AGARD-R-780. In addition, Polito's [4] approach, relative to the spectral solution of the inverse problem for airfoils, and that of Bauer *et al*. [5] for shockless airfoils, should be mentioned. One drawback of inverse problems is that they may be ill posed, as certain wall pressure distributions on airfoils result in open or self-intersecting profiles. Lighthill [2] discovered the solvability conditions that should be respected by pressure distributions within an incompressible potential flow model, whereas the solvability conditions for compressible flows were investigated in [6] and references therein.

The appeal of the inverse problem solution for aerodynamic design declined as powerful computers and sound numerical methods that allow numerical optimization of aerodynamic components became available. Once a functional that defines the relative merit or cost of a certain solution is defined, a numerical optimization algorithm can be as simple as (i) computing the functional gradient relative to the controls by divided differences, (ii) marching toward the functional extremum using gradient information. If the number of parameters that have to be optimized is in fact not very small, finding the gradient requires a huge amount of computational time. The computation of each gradient component needs a flow evaluation, making optimizations using the Euler or Navier–Stokes models unfeasible.

Greater computational efficiency is obtained by using the adjoint method (see [7–9]) to compute the functional gradient. Evaluation of the gradient requires one adjoint calculation and one flow calculation, regardless of the number of design variables. This approach has opened up the possibility of optimizing tridimensional compressible viscous flows over wing–body configurations at high Reynolds numbers; see [10].

The advantages of numerical optimization over the inverse problem can be summarized in that numerical optimization allows the maximization or minimization of global quantities such as lift or drag in the presence of constraints, whereas for inverse problems the design is limited to the pressure distribution selection on the boundary, which is given on the basis of designer experience and is therefore somewhat arbitrary. In addition, no control of the final geometry is possible. In this work we try to overcome these weaknesses by extending the adjoint optimization method to inverse problems.

To formulate a shape optimization problem we need a functional $\mathcal{F}$ to be either minimized or maximized. We have $\mathcal{F} = \mathcal{F}[U(\Gamma), \Gamma]$ where U is the flow variables vector and Γ represents the geometry. In the adjoint method such an extremum problem is solved using a variational technique and introducing a Lagrange multiplier vector Λ dual of the flow variables vector. Using the Lagrange multipliers we are able to write $\delta\mathcal{F}$ for $\Gamma \leftarrow \Gamma + \delta\Gamma$, at the cost of solving a system of partial differential equations (PDEs) for the Lagrange multipliers which is the mathematical adjoint of the governing equations. Once the gradient is known, the initial geometry is perturbed accordingly and the procedure is started all over again until a convergence criterion is satisfied.

The adjoint method can be adapted to an inverse problem formulation. Let $p(s)$ be the flow quantity we prescribe on the flow-field boundary, where for example p is the pressure and s is the curvilinear coordinate along the boundary. We define a cost/merit functional in much the same way as before: $\mathcal{F} = \mathcal{F}[U(p), p]$. It should be noted that the control is now the pressure distribution on the boundary, whereas in usual adjoint methods the control is the boundary shape. The derivation of the adjoint follows the same steps as in the shape optimization case, to finally obtain $\delta\mathcal{F}$ for $p(s) \leftarrow p(s) + \delta p(s)$. The pressure distribution is then altered according to the gradient information until the extremum is eventually reached. In this formulation the boundary shape results from the

solution of the inverse problem corresponding to each optimization step. In this respect the optimization of an inverse problem can be considered a *flow design optimization* as opposed to the optimization of a direct problem, which is known as *shape design optimization*. The idea of optimizing the pressure distribution is not new; it was proposed in [11] with the motivation that "this procedure avoids most if not all of the limitations of the pure inverse method."

Flow design optimization offers a very simple way of implementing flow constraints, as they can be directly included in the parameterization of the control. Inevitably, in the design process it is necessary to focus on a given model to account for the physically relevant phenomena which affect performance. Yet, it is mandatory to include results obtained by more sophisticated models or other disciplines, in the selected model. These results usually take the form of constraints on the governing equation variables, and not on the geometry. For example, let us consider a propeller to be designed to maximize traction for given shaft work. The selected model is that of an inviscid compressible fluid governed by the compressible Euler equations, a model that is appropriate to compute the traction of a propeller. However, one must also take into account the constraints on the emitted noise. These requirements may have the form of constraints on the load of the propeller blades, which in turn is a function of the flow variables at the wall. Therefore any time we have a design problem where the effects that are not represented in the governing equations are to be considered, the optimization based on the solution of the inverse problem adjoint equations is a natural way of formulating the problem.

For example, in the numerical tests, a diffuser is studied where the pressure distribution at the wall is optimized for minimal axial deviation at the outlet. The maximum attainable pressure gradient is constrained in order to avoid premature flow detachment. In the usual adjoint optimal shape design formulation, flow constraints are accounted for either through additional Lagrange multipliers, which means there are additional PDEs to be solved, or by a penalization in the functional. For the method proposed here, the situation is reversed: Geometric constraints result in either additional PDEs or in functional penalization. Hence, for example, the inverse problem closure and univalence conditions for airfoils are bypassed by imposing appropriate geometric constraints on the solution.

In the following, the problem is formulated and the gradient is derived in detail for two applications which are solved using an inverse problem. The first example is intended to make the ideas clear. We then concentrate on a case that is complicated by a flow model which describes a turbo fan stage. As previously mentioned, the first case concerns the problem of designing a diffuser. We wish to determine the wall pressure distribution so that the flow axial deviation at the outlet is at a minimum, with constraints on the allowed wall pressure gradient.

The second example is more oriented to applications and is related to a flow model of a complete piece of turbo-machinery; see [13]. The blades of the turbo-machinery are modeled as flow surfaces of zero thickness which exert forces on the fluid flow. This approximation introduces volume forces in the compressible Euler equations, which is the model adopted for the flow. Our method is such that, instead of modifying the shape of the flow surfaces that model the blades, we give the force that the blades exert on the flow and let the geometry accommodate this distribution of forces. The volume force distribution itself is modified according to the functional gradient, so that, for example, thrust is maximized.

2. DIFFUSER WITH MINIMAL AXIAL DEVIATION AT THE OUTLET

Let us consider a two-dimensional diffuser with total pressure, total temperature, and flow angles imposed at the inlet; pressure is given at the outlet. The walls of the diffuser should be designed so that the flow at the outlet has minimal axial deviation and the diffuser causes a given pressure rise with a constraint on the maximum wall pressure gradient. The constraint imposed qualitatively reflects the Stratford [14] semiempirical separation criterion for decelerated turbulent boundary layers,

$$c_p \sqrt{s \frac{dc_p}{ds}} = C s^{\frac{1}{10}}, \tag{1}$$

where C is a constant function of the Reynolds number per unit length, s is the wall curvilinear coordinate, and c_p is the pressure coefficient. We take $s \approx x$ and $c_p = 2\frac{p - p_{in}}{\rho U_{in}^2}$, where in refers to the inlet section. As the dynamic pressure is approximately equal to the difference between the total pressure p^0 and the inlet pressure p_{in}, we obtain $\frac{dp}{dx} \approx \frac{dc_p}{dx}(p^0 - p_{in})$. The maximum allowable pressure gradient at the wall $\Pi(x)$ is displayed in Fig. 1. In addition, the gradient is also required to be positive. This simple problem can be encountered in the design of wind tunnel diffusers, air-breathing engine intakes, or turbo-machine casings.

2.1. Flow Model and Inverse Problem Solution Method

The flow is governed by the two-dimensional compressible Euler equations. In Cartesian coordinates (x, y), one has

$$\frac{\partial \mathbf{U}}{\partial t} + \frac{\partial \mathbf{F}}{\partial x} + \frac{\partial \mathbf{G}}{\partial y} = 0, \tag{2}$$
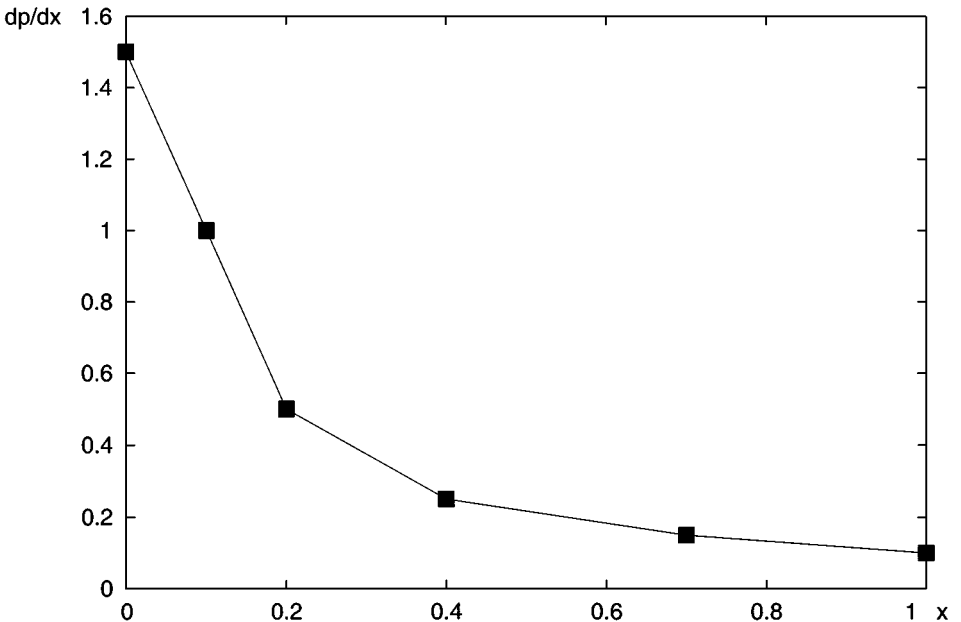

FIG. 1. Constraint on the pressure gradient along the x-axis.

where

$$\mathbf{U} = \left\{ \begin{array}{c} \rho \\ \rho u \\ \rho w \\ e \end{array} \right\} \quad \mathbf{F} = \left\{ \begin{array}{c} \rho u \\ p + \rho u^2 \\ \rho u w \\ u(p + e) \end{array} \right\} \quad \mathbf{G} = \left\{ \begin{array}{c} \rho w \\ \rho u w \\ p + \rho w^2 \\ w(p + e) \end{array} \right\},$$

and as usual, ρ is the density, p is the pressure, and e is the total internal energy per unit volume. The diffuser geometry is unknown, but it is obtained by imposing a given pressure distribution $p = p_e(s)$ on the solid boundaries, as opposed to direct problems where the geometry is known and the no-through-flow condition applies on the diffuser walls. In this sense, for the sake of conciseness, we can write Eq. 2 as $\mathbf{E}(\mathbf{U}, p_e) = 0$.

This solution method is based on the ideas presented in [15] and [16]. The diffuser walls can be considered deformable and impermeable surfaces fastened to the diffuser inlet section that move under the effect of the imposed pressure. An initial wall configuration is guessed. The resulting transient is described by integrating the equations that govern the time-dependent flow motion. The results differ from those of a usual flow solver in two ways. The first is that the no-through-flow boundary condition at the wall is replaced by a condition of given pressure; the second is that the number of equations that must solved is increased by one, the kinematic equation governing the surface motion. This equation is obtained by imposing the condition that the speed of the moving wall must be locally equal to the normal flow velocity. Therefore, in terms of computational cost, the inverse problem solution is equivalent to a direct solution.

A finite volume formulation, based on the approximate Riemann solver [17] to compute the fluxes at cell interfaces, is applied. Second-order spatial accuracy is obtained using an ENO class method [18]. At the end of the transient, the walls assume the shape that solves the inverse problem, i.e., find the shape which induces the given pressure distribution on the walls.

2.2. Variational Formulation, Adjoint Equations, and Gradient

The wall pressure $p_e(s)$ that should be imposed on the diffuser walls which minimize the functional

$$D[p_e(s)] = \frac{1}{2} \int_{out} \left(\frac{w}{u} \right)^2 dy \tag{3}$$

has to be determined. In order to solve such a constrained extremum problem, we introduce the Lagrangian function

$$\mathcal{L}(\mathbf{U}, p_e, \Lambda) = D + \int_{\Omega} {}^t\Lambda \mathbf{E}(\mathbf{U}, p_e) \, d\Omega, \tag{4}$$

where ${}^t\Lambda(x, y) = \{\lambda_1, \lambda_2, \lambda_3, \lambda_4\}$ are Lagrange multipliers. This approach allows us to treat the problem as unconstrained. A stationary configuration is found when the variation of $\mathcal{L}$ with respect to all its arguments, which are now considered independent functions, is 0. Computing $\delta\mathcal{L}$ as in [20], we obtain

$$\delta\mathcal{L} = \delta\mathcal{L}_U + \delta\mathcal{L}_{p_e} + \delta\mathcal{L}_\Lambda \tag{5}$$

with

$$\delta\mathcal{L}_U = \delta D_U + \int_{\Sigma} {}^t\Lambda(\mathbf{F}_U n_x + \mathbf{G}_U n_y)\delta\mathbf{U}\, d\sigma - \int_{\Omega} ({}^t\Lambda_x \mathbf{F}_U + {}^t\Lambda_y \mathbf{G}_U)\delta\mathbf{U}\, d\Omega, \quad (6)$$

where Σ is the boundary of flow field Ω, and $\mathbf{F}_U$, $\mathbf{G}_U$ are the Jacobian matrices of $\mathbf{F}$ and $\mathbf{G}$.

All contributions to $\delta\mathcal{L}$ must be 0 at the maximum. Hence, to find a stationary point, we enforce

$$\delta\mathcal{L}_U = 0 \quad \delta\mathcal{L}_\Lambda = 0.$$

In general this results in $\delta\mathcal{L}_{p_e} \neq 0$. To reach the minimum, we take δp_e so that $\delta\mathcal{L} = \delta\mathcal{L}_{p_e} < 0$. It should be noted that the variations of $\mathcal{L}$ with respect to the Lagrange multipliers Λ simply yield the flow equations.

From the condition $\delta\mathcal{L}_U = 0$, the adjoint of the Euler equations and its boundary conditions are obtained.

$${}^t\Lambda_x \mathbf{F}_U + {}^t\Lambda_y \mathbf{G}_U = 0 \text{ in } \Omega \tag{7}$$

and

$$\left[\frac{w}{u}\frac{\partial}{\partial\mathbf{U}}\left(\frac{w}{u}\right)h(\Sigma) + {}^t\Lambda(\mathbf{F}_U n_x + \mathbf{G}_U n_y) \right]\delta\mathbf{U} = 0 \text{ on } \Sigma, \tag{8}$$

where $h(\Sigma)$ is 1 at the outlet and 0 elsewhere. The previous relation requires additional interpretation according to the flow equation boundary conditions. For the inlet and outlet boundary conditions, see Eq. (43) for a similar case. The wall adjoint boundary condition is peculiar to this problem and is hereafter considered.

Let us consider Eq. (8). At the moving wall, $\delta\mathbf{U}$ can be written in terms of only three independent variations, as $\delta p_e(s) = 0$. We take $\delta(\rho e)$ as the dependent variation and obtain

$$(\mathbf{F}_U n_x + \mathbf{G}_U n_y)\delta\mathbf{U} = \begin{Bmatrix} 0 & n_x & n_y \\ 0 & un_x & un_y \\ 0 & wn_x & wn_y \\ 0 & n_x(e+p)/\rho & n_y(e+p)/\rho \end{Bmatrix} \begin{Bmatrix} \delta\rho \\ \delta(\rho u) \\ \delta(\rho v) \end{Bmatrix},$$

where we take into account that the wall velocity is 0 when the inverse problem solution is attained. Equation (8), then, translates into the single condition

$$\lambda_1 + u\lambda_2 + w\lambda_3 + \frac{e+p}{\rho}\lambda_4 = 0 \tag{9}$$

that has to be satisfied at the wall. The functional gradient is

$$\delta D_{p_e} = \int_{wall} (\lambda_2 n_x + \lambda_3 n_y)\delta p\, ds. \tag{10}$$

2.2.1. *Pressure Parameterization*

The diffuser has imposed inlet p_{in} and outlet p_{out} wall pressures. The distributed control is the wall pressure gradient. On the discrete level, the pressure is recovered as

$$p_e(x_i) = p_{in} + \sum_{j=2}^{i} m(x_j)\Delta x_j, \quad m(x_j) = \left(\frac{dp_e}{dx}\right)_j \tag{11}$$

with the constraint

$$\sum_{j=2}^{N} m(x_j)\Delta x_j = p_{out} - p_{in} \tag{12}$$

to match the exit pressure. Δx_j is the grid size in the x-direction and N is the number of computational points in the x-direction. We have $N - 1$ control parameters represented by the pressure gradient at the discretization points.

Let us consider Eq. (10) and discretize it as

$$\delta D_{p_e} = \sum_{j=2}^{N} \chi_j \delta p_j, \tag{13}$$

with $\chi_j = [(\lambda_2 n_x + \lambda_3 n_y)\Delta s]_j$ and $\delta p_j = \sum_{i=2}^{j} \delta m(x_i)\Delta x_i$. We have

$$\delta D_{p_e} = \sum_{i=2}^{N} \delta m(x_i)\Delta x_i \sum_{j=i}^{N} \chi_j. \tag{14}$$

Take $\psi_i = \Delta x_i \sum_{j=i}^{N} \chi_j$. If there were no constraints on the pressure gradient, we could simply set $\delta m(x_i) = -\varrho \psi_i$ to obtain $\delta D < 0$. Yet, in view of Eq. (12), we also obtain

$$\sum_{i=2}^{N} \varphi_i \delta m(x_i)\Delta x_i = 0. \tag{15}$$

If $0 \le m(x_i) \le \Pi(x_i)$, then $\varphi_i = 1$; otherwise we take $\delta m(x_i) = 0$ and $\varphi_i = 0$. By projecting the gradient onto the plane tangent to the constraints (see Fig. 2) we have $\delta D < 0$ by taking

$$\{\phi_i\} \times \{\psi_i\} \times \{\phi_i\} = \delta m(x_i) = \varrho \left(\psi_i \sum_{j=2}^{N} \varphi_j^2 - \varphi_i \sum_{j=2}^{N} \psi_j \varphi_j \right). \tag{16}$$

The solution of the optimization problem is achieved by initializing the coefficients $m(x_j)$, computing the corresponding wall geometry using the inverse problem, solving the adjoint equations, and updating the coefficients $m(x_j)$, according to the projected gradient, until the minimum is reached.
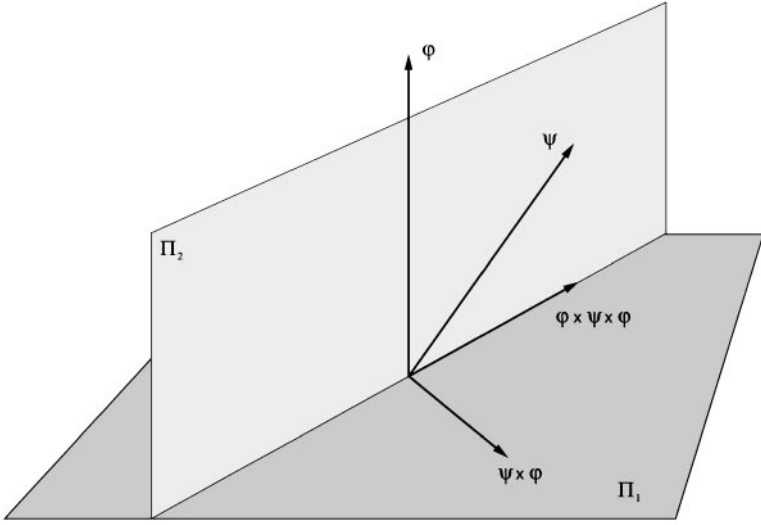
FIG. 2. Projection of the gradient onto the constraint space.

2.3. Comparison with Classical Adjoint Formulation

The same problem can be solved by an adjoint formulation where the controls are the position of the upper boundary discretization points. In such a case, the functional to be minimized is

$$D_1[\Gamma_w] = \frac{1}{2} \int_{out} \left(\frac{w}{u} \right)^2 dy, \tag{17}$$

where Γ_w is the upper wall. The solution to such a problem would be a straight duct, however, leading to the same pressure at the inlet and outlet. In order to accomplish a certain pressure increase between the inlet and outlet it is also necessary to require that

$$D_2[\Gamma_w] = \left(p_{in}^w - p_{in}^* \right)^2 = \int_{\Gamma_w} [p^w(\Gamma_w) - p_{in}^*]^2 f(\Gamma_w) \, d\Gamma_w$$

be minimized, where p_{in}^w is the actual wall pressure at the inlet, p_{in}^* is the desired pressure, and $f(\Gamma_w)$ is the Dirac delta centered at the inlet. The outlet pressure is imposed in the flow equation boundary conditions.

In addition, the pressure gradient at the upper wall must be bounded from above by a certain distribution $g_{max}(\Gamma_w)$, for example, the Stratford distribution. We also want to avoid negative pressure gradients, as in the case in the previous sections. Therefore we have two additional functionals to minimize:

$$D_3[\Gamma_w] = \left(\frac{dp}{dx} - g_{max} \right)^2 + \left| \frac{dp}{dx} - g_{max} \right| \left(\frac{dp}{dx} - g_{max} \right)$$

and

$$D_4[\Gamma_w] = \left(\frac{dp}{dx} \right)^2 - \left| \frac{dp}{dx} \right| \left(\frac{dp}{dx} \right).$$

The way to deal with such additional constraints is usually to penalize the original functional to also minimize the additional terms. The Lagrangian becomes

$$\mathcal{L}(\mathbf{U}, \Gamma_w, \Lambda) = \sum_{i=1}^{4} \varpi_i D_i + \int_{\Omega} {}^t\Lambda \mathbf{E}(\mathbf{U}, \Gamma_w) \, d\Omega + \int_{\Gamma_w} \mu(\rho(un_x + vn_y)) \, d\Gamma_w, \quad (18)$$

where ϖ_i are arbitrarily chosen weights and μ is an additional Lagrange multiplier to account for the no-through-flow condition. It is well known that such functionals lead to ill conditioned optimization problems resulting in very time-consuming or unfeasible calculations. Further discussion of the penalization approach and alternate approaches can be found in [12].

Let us forget the pressure gradient bounds and consider a problem where only D_2 is present. We want to find the shape of a diffuser so that it causes a certain pressure increase. Since the outlet is allowed to change dimension, the optimization becomes very stiff. This is intuitively understood as follows. Let the initial configuration be a constant section duct, so that the pressure is constant and equal to the outlet value. Since $p_{in}^* < p_{out}$ we have two contrasting effects. Lowering the wall locally, we would obtain a pressure decrease and consequently a decrease in D_2. On the other hand, the wall must rise to accommodate a global section increase which determines a pressure decrement at the inlet, for a given outlet pressure. The authors have in fact tested a usual adjoint code [20] for this simple problem. By using a conjugate gradient descent method without line search, we were only able to attain a gradient reduction of about two orders of magnitude after 10,000 optimization steps! Nozzle results presented in the literature, e.g., [19] and [20], show similar stiff behavior even if the optimization problem is simpler, as the outlet geometry is fixed.

3. FAN STAGE WITH MAXIMUM THRUST

The fan of a turbojet engine is composed of a rotor that raises the total pressure of the flow and a stator to deflect the flux. We want to determine, using a simplified flow model, the rotor and stator geometries that result in maximum thrust of the fan, for a given amount of work performed on the fluid.

3.1. Turbo-machine Flow Model in the Meridional Plane

The flow deflection through the rotors and stators of a turbo-machine is the result of the forces that rotor and stator blades exert on the flow. An axisymmetric model of a turbo-machine can be set up by replacing the blade rows with volume forces. It is assumed that the blade rows have vanishing thickness and infinite solidity, so that the single blade coincides with a stream surface. Thus, in the case of an inviscid flow, the effect of solid blades is modeled by volume forces orthogonal to the stream surfaces.

Let

$$\mathbf{F} = F^x \mathbf{i} + F^r \xi + F^\vartheta \eta \quad (19)$$

be the volume force, where $\mathbf{i}$, ξ, and η are the unit vectors that are pertinent to the axial, radial, and tangential directions in cylindrical coordinates $(x\mathbf{i}, r\xi, \vartheta\eta)$. The distribution

of the tangential component $F^\vartheta = F^\vartheta(x, r)$ is the function that has to be optimized, the same way that the shape of a wall is usually optimized in common optimization algorithms.

The geometry of the blades, represented by 2D manifolds

$$\Theta(x, r, \vartheta) = 0 \tag{20}$$

is found by solving

$$(\mathbf{q} - j\omega r\eta) \cdot \nabla\Theta = 0 \tag{21}$$

since the blades are considered stream surfaces of the absolute or relative motion for the stators and rotors, respectively. In the previous equation, $\mathbf{q} = u\mathbf{i} + w\xi + v\eta$ is the flow velocity vector, ω is the angular velocity of the rotors, and $j = 0$ for the stators, $j = 1$ for the rotors.

The components of the volume force F^x and F^r are determined by enforcing the condition that the blade manifolds be orthogonal to the volume forces

$$\mathbf{F} \times \nabla\Theta = 0, \tag{22}$$

which implies

$$F^x = r\frac{\Theta_x}{\Theta_\vartheta} F^\vartheta \tag{23}$$

and

$$F^r = r\frac{\Theta_r}{\Theta_\vartheta} F^\vartheta. \tag{24}$$

3.2. Inverse Problem

In this section details are given of the solution technique of the inverse problem considering $F^\vartheta(x, r)$ as known. It should be noted that the distribution $F^\vartheta(x, r)$ is updated during the optimization in order to maximize the cost function.

The solution method is based on the ideas presented in [13–16] and is based on a time-dependent process. The blades can be seen as deformable and impermeable surfaces constrained at the leading edge. They move like fastened sails waving under the effect of the wind. An initial configuration of such surfaces is guessed. The subsequent transient is described by integrating the equations governing the time-dependent flow motion. At the end of the transient, the blades assume the shape that solves the inverse problem.

In cylindrical coordinates, the compressible Euler equations with volume forces acting on the fluid are

$$\frac{\partial \mathbf{U}}{\partial t} + \frac{\partial \mathbf{A}}{\partial x} + \frac{\partial \mathbf{B}}{\partial r} + \mathbf{Q} = 0, \tag{25}$$

where

$$\mathbf{U} = \left\{ \begin{array}{c} \rho \\ \rho u \\ \rho v \\ \rho w \\ e \end{array} \right\} \quad \mathbf{A} = \left\{ \begin{array}{c} \rho u \\ p + \rho u^2 \\ \rho u v \\ \rho u w \\ u(p+e) \end{array} \right\} \quad \mathbf{B} = \left\{ \begin{array}{c} \rho w \\ \rho u w \\ \rho v w \\ p + \rho w^2 \\ w(p+e) \end{array} \right\}$$

$$\mathbf{Q} = \left\{ \begin{array}{c} \frac{\rho w}{r} + \rho u \alpha \\ \frac{\rho u w}{r} - F^x + \rho u^2 \alpha \\ 2\frac{\rho v w}{r} - F^\theta \\ \frac{\rho(v^2 - w^2)}{r} - F^r \\ \frac{w(p+e)}{r} - \mathbf{F} \cdot \mathbf{q} + u(p+e)\alpha \end{array} \right\}.$$

The boundary conditions at the entry section are the flow angles, the total pressure, and the total temperature when the flow is subsonic, while all the flow properties are prescribed if the flow is supersonic; at the exit section, the static pressure is prescribed if the flow is subsonic, while no boundary conditions are needed when the flow is supersonic. The blockage caused by the blades is taken into account by the terms containing the coefficient α, with

$$\alpha = \frac{\partial (\log \Xi)}{\partial x}$$

and with Ξ being the free passage per unit radius,

$$\Xi = 2\pi r - T,$$

where $T = T(x, r)$ is the sum of the estimated blade thickness, including the boundary layers.

The system of Eq. (25) is integrated in time using a finite volume formulation based on an approximate Riemann solver [17] to compute the fluxes at the cell interfaces. Second-order spatial accuracy is obtained using an ENO class method [18].

A blade surface changes shape during the transient to obey the impermeable wall condition. Let us express Eq. (20) as

$$\Theta(x, r, \vartheta, t) = \vartheta - g(x, r, t) = 0 \tag{26}$$

so that Eqs. (23) and (24) become

$$F^x = -rg_x F^\vartheta \tag{27}$$

$$F^r = -rg_r F^\vartheta. \tag{28}$$

Flow particles on $\Theta(x, r, \vartheta, t) = 0$ must remain on the manifold for the impermeable wall condition. It follows that, during the transient, the Langragian derivative of the function $\Theta(x, r, \vartheta, t)$ has to be null,

$$\frac{d\Theta}{dt} = \Theta_t + (q - j\omega r\eta) \cdot \nabla\Theta = 0 \tag{29}$$

that can be written as

$$g_t = -ug_x - wg_r + \frac{v - j\omega r}{r}, \tag{30}$$

with $j = 0$ for stators and $j = 1$ for rotors. The above equation is solved coupled to the Euler equations, and it is integrated in time upwinding the spatial derivatives of g according to u and w.

3.3. Flow Equations Adjoint

The functional we consider is the conventional thrust expressed as

$$T(F^\vartheta) = \left[\int_{r_h}^{r_t} (p + \rho u^2) r \, dr\right]_{out} - \left[\int_{r_h}^{r_t} (p + \rho u^2) r \, dr\right]_{in} = \int_{\Gamma_{io}} H(U) \, d\Gamma, \tag{31}$$

where F^ϑ is the control, while r_t and r_h are the tip and hub radius, respectively. The maximum of T is constrained by the steady state Euler equations

$$\mathbf{E}(F^\vartheta) = \mathbf{A}_x + \mathbf{B}_r + \mathbf{Q} = 0 \tag{32}$$

and by the kinematic constraint on the blades

$$\mathbf{G}(\mathbf{U}(F^\vartheta)) = ug_x + wg_r - \frac{v - j\omega r}{r} = 0. \tag{33}$$

We introduce the Lagrangian function

$$\mathcal{L}(\mathbf{U}, g, F^\vartheta, \Lambda, \mu) = \int_{\Gamma_{io}} \mathbf{H}(\mathbf{U}) \, d\Gamma + \int_\Omega {}^t\Lambda \mathbf{E}(\mathbf{U}, F^\vartheta, g) \, d\Omega + \int_\Omega \mu G(\mathbf{U}, g) \, d\Omega, \tag{34}$$

where ${}^t\Lambda(x, r) = \{\lambda_1, \lambda_2, \lambda_3, \lambda_4, \lambda_5\}$ and $\mu = \mu(x, r)$ are Lagrange multipliers. Let us compute $\delta\mathcal{L}$. We have

$$\delta\mathcal{L} = \delta\mathcal{L}_U + \delta\mathcal{L}_{F^\vartheta} + \delta\mathcal{L}_g + \delta\mathcal{L}_\Lambda + \delta\mathcal{L}_\mu, \tag{35}$$

with

$$\delta\mathcal{L}_U = \int_{\Gamma_{io}} \frac{\partial \mathbf{H}}{\partial \mathbf{U}} \delta\mathbf{U} \, d\Gamma + \int_\Omega {}^t\Lambda \delta\mathbf{E}_U \, d\Omega + \int_\Omega \mu \frac{\partial G}{\partial \mathbf{U}} \delta\mathbf{U} \, d\Omega \tag{36}$$

$$\delta\mathcal{L}_\Lambda = \int_\Omega {}^t\delta\Lambda \mathbf{E}(\mathbf{U}, F^\vartheta, g) \, d\Omega \tag{37}$$

$$\delta\mathcal{L}_\mu = \int_\Omega G(\mathbf{U}, g)\delta\mu \, d\Omega \tag{38}$$

$$\delta\mathcal{L}_{F^\vartheta} = \int_\Omega {}^t\Lambda \frac{\partial \mathbf{Q}}{\partial F^\vartheta} \delta F^\vartheta \, d\Omega \tag{39}$$

$$\delta\mathcal{L}_g = \int_\Omega {}^t\Lambda \delta\mathbf{Q}_g \, d\Omega + \int_\Omega \mu \delta G_g \, d\Omega. \tag{40}$$

The vectors $\frac{\partial \mathbf{Q}}{\partial F^{\vartheta}}$ and $\frac{\partial G}{\partial \mathbf{U}}$ are easily computed; $\frac{\partial \mathbf{H}}{\partial \mathbf{U}}$ is the derivative of the difference of the flux component in the x-direction, taken at the inlet and outlet sections.

The single contributions of $\delta \mathcal{L}$ must be 0 at the maximum. At the stationary point we enforce

$$\delta \mathcal{L}_U = 0 \quad \delta \mathcal{L}_\Lambda = 0 \quad \delta \mathcal{L}_\mu = 0 \quad \delta \mathcal{L}_g = 0.$$

In general this results in $\delta \mathcal{L}_{F^{\vartheta}} \neq 0$. To reach the maximum we take δF^{ϑ} so that $\delta \mathcal{L} = \delta \mathcal{L}_{F^{\vartheta}} > 0$, for example using a conjugate gradient method, as explained in the following.

We can manipulate Eq. (35), obtaining

$$\delta \mathcal{L}_U = \int_{\Gamma_{io}} \frac{\partial \mathbf{H}}{\partial \mathbf{U}} \delta \mathbf{U} \, d\Gamma + \int_\Sigma {}^t\Lambda (\mathbf{A}_U n_x + \mathbf{B}_U n_r) \delta \mathbf{U} \, d\sigma - \int_\Omega ({}^t\Lambda_x \mathbf{A}_U + {}^t\Lambda_r \mathbf{B}_U) \delta \mathbf{U} \, d\Omega$$
$$+ \int_\Omega {}^t\Lambda \frac{\partial \mathbf{Q}}{\partial \mathbf{U}} \delta \mathbf{U} \, d\Omega + \int_\Omega \mu \frac{\partial G}{\partial \mathbf{U}} \delta \mathbf{U} \, d\Omega, \tag{41}$$

where Σ is the entire border of the flow field Ω, and $\mathbf{A}_U$, $\mathbf{B}_U$, and $\mathbf{Q}_U$ are Jacobian matrices. From the condition $\delta \mathcal{L}_U = 0$ we obtain the adjoint of the flow equations and the relative boundary conditions; that is,

$$ {}^t\Lambda_x \mathbf{A}_U + {}^t\Lambda_r \mathbf{B}_U - {}^t\Lambda \frac{\partial \mathbf{Q}}{\partial \mathbf{U}} - \mu \frac{\partial G}{\partial \mathbf{U}} = 0 \text{ in } \Omega \tag{42}$$

and

$$\left[\frac{\partial \mathbf{H}^*}{\partial \mathbf{U}} + {}^t\Lambda (\mathbf{A}_U n_x + \mathbf{B}_U n_r) \right] \delta \mathbf{U} = 0 \text{ on } \Sigma, \tag{43}$$

where $H^* = H$ for the inlet and the outlet, and $H^* = 0$ elsewhere.

The condition $\delta \mathcal{L}_g = 0$ yields

$$\delta \mathcal{L}_g = \int_{\Omega_b} \mu \delta G_g \, d\Omega + \int_{\Omega_b} {}^t\Lambda \delta \mathbf{Q}_g \, d\Omega$$
$$= \int_{\Sigma_b} \mu (\mathbf{q} \cdot \mathbf{n}) \delta g \, d\sigma - \int_{\Omega_b} [(\mu u)_x + (\mu w)_r] \delta g \, d\Omega + \int_{\Omega_b} {}^t\Lambda \delta \mathbf{Q}_g \, d\Omega = 0, \tag{44}$$

where it should be noted that the domain of integration Ω_b and the bounding curve Γ_b are those relative to the blades. The last integral in the above equation is

$$\int_{\Omega_b} {}^t\Lambda \delta \mathbf{Q}_g \, d\Omega = \int_{\Omega_b} {}^t\Lambda \mathbf{K} \nabla (\delta g) \, d\Omega = \int_{\Sigma_b} ({}^t\Lambda \mathbf{K}) \cdot \mathbf{n} \, \delta g \, d\sigma - \int_{\Omega_b} \nabla \cdot ({}^t\Lambda \mathbf{K}) \delta g \, d\Omega, \tag{45}$$

where $\mathbf{n} = (n_x, n_y)$ and

$$\mathbf{K} = r F^{\vartheta} \begin{Bmatrix} 0 & 0 \\ 1 & 0 \\ 0 & 0 \\ 0 & 1 \\ u & w \end{Bmatrix}.$$

Hence, the adjoint of the kinematic constraint is

$$(\mu u)_x + (\mu w)_r - \nabla \cdot ({}^t\Lambda \mathbf{K}) = 0 \text{ in } \Omega_b \tag{46}$$

and

$$[\mu(\mathbf{q} \cdot \mathbf{n}) + ({}^t\Lambda \mathbf{K}) \cdot \mathbf{n}] \, \delta g = 0 \text{ on } \Gamma_b, \tag{47}$$

which yields the boundary conditions for Eq. (46) as explained in the following. The adjoint equation of the kinematic constraint is coupled to Eq. (42) the same way the kinematic constraint is coupled to the flow equations.

It should be noted that the variations of $\mathcal{L}$ with respect to Λ and μ simply yield the flow equations and the kinematic constraint respectively.

Finally, we are left with

$$\delta\mathcal{L} = \delta\mathcal{L}_{F^\vartheta} = \int_{\Omega_b} {}^t\Lambda \frac{\partial \mathbf{Q}}{\partial F^\vartheta} \delta F^\vartheta \, d\Omega. \tag{48}$$

This functional depends on $\mathbf{U}$, Λ, μ; these are variables that satisfy the flow equations, the kinematic constraint, and the respective adjoints. Therefore, if we update the present distribution of F^ϑ with

$$\delta F^\vartheta = \varrho \, {}^t\Lambda \frac{\partial \mathbf{Q}}{\partial F^\vartheta},$$

taking $\varrho > 0$, then $\delta\mathcal{L} > 0$. By iterating such a procedure, the maximum is eventually reached.

This method, namely the gradient method, has a very slow convergence rate. Better convergence rates are obtained with the conjugate gradient method [21], in which the correction to F^ϑ at the iterate k is

$$(\delta F^\vartheta)^k = \varrho \left[\left({}^t\Lambda \frac{\partial \mathbf{Q}}{\partial F^\vartheta} \right)^k - \beta^{k-1} (\delta F^\vartheta)^{k-1} \right],$$

with

$$\beta^{k-1} = \frac{\int_{\Omega_b} \left[\left({}^t\Lambda \frac{\partial \mathbf{Q}}{\partial F^\vartheta} \right)^k - \left({}^t\Lambda \frac{\partial \mathbf{Q}}{\partial F^\vartheta} \right)^{k-1} \right] \left({}^t\Lambda \frac{\partial \mathbf{Q}}{\partial F^\vartheta} \right)^k d\Omega}{\int_{\Omega_b} \left[\left({}^t\Lambda \frac{\partial \mathbf{Q}}{\partial F^\vartheta} \right)^{k-1} \right]^2 d\Omega}.$$

3.3.1. Inlet Boundary Conditions

Let $\mathbf{n} = (0, -1, 0)$ at the inlet, so that Eq. (43) reduces to

$$\frac{\partial \mathbf{H}^*}{\partial \mathbf{U}} \delta \mathbf{U} - {}^t\Lambda \frac{\partial \mathbf{A}}{\partial \mathbf{U}} \delta \mathbf{U} = 0. \tag{49}$$

As the flow variables $\mathbf{U}$ have given conditions at the boundaries, the variation $\delta \mathbf{U}$ at the inlet is such that the boundary conditions on $\mathbf{U}$ are still satisfied. For example, if the inlet flow is supersonic, all of the components of $\mathbf{U}$ are given. In this case $\delta \mathbf{U} = 0$ and consequently there is no boundary condition on Λ.

In the case of subsonic inlet, four boundary conditions must be provided, for example,

$$dS = 0, \quad dT^o = 0, \quad d\sigma = 0, \quad d\epsilon = 0, \tag{50}$$

where

$$S = \log \frac{p}{\rho} - 2\kappa \log \rho \tag{51}$$

$$T^o = \frac{p}{\rho} + \frac{\kappa}{\gamma}(u^2 + v^2 + w^2) = -\frac{2\kappa^2}{\gamma}V^2 + 2\kappa\frac{u_5}{u_1} \tag{52}$$

$$\sigma = \frac{v}{u} = \frac{u_3}{u_2}, \quad \epsilon = \frac{w}{u} = \frac{u_4}{u_2}, \tag{53}$$

where we set $\mathbf{U} = (\rho, \rho u, \rho v, \rho w, e) = (u_1, u_2, u_3, u_4, u_5)$; $\kappa = \frac{\gamma-1}{2}$; and γ is the specific heat ratio. We have

$$\begin{cases} \delta S = \frac{\partial S}{\partial u_1}\delta u_1 + \frac{\partial S}{\partial u_2}\delta u_2 + \frac{\partial S}{\partial u_3}\delta u_3 + \frac{\partial S}{\partial u_4}\delta u_4 + \frac{\partial S}{\partial u_5}\delta u_5 = 0 \\[2mm] \delta T = \frac{\partial T}{\partial u_1}\delta u_1 + \frac{\partial T}{\partial u_2}\delta u_2 + \frac{\partial T}{\partial u_3}\delta u_3 + \frac{\partial T}{\partial u_4}\delta u_4 + \frac{\partial T}{\partial u_5}\delta u_5 = 0 \\[2mm] \delta \sigma = \frac{\partial \sigma}{\partial u_2}\delta u_2 + \frac{\partial \sigma}{\partial u_3}\delta u_3 = 0 \\[2mm] \delta \epsilon = \frac{\partial \epsilon}{\partial u_2}\delta u_2 + \frac{\partial \epsilon}{\partial u_4}\delta u_4 = 0. \end{cases} \tag{54}$$

By selecting δu_2 as the independent variation, we obtain

$$\delta \mathbf{U} = \begin{Bmatrix} \frac{u_1 V^2}{u_2((1+\gamma\kappa)V^2 - 2\gamma\kappa u_1 u_5)} \\[2mm] 1 \\[2mm] \frac{u_3}{u_2} \\[2mm] \frac{u_4}{u_2} \\[2mm] \frac{V^2((1-4\kappa^2)u_1 u_5 + 2\kappa^2 V^2)}{u_1 u_2((1+\gamma\kappa)V^2 - 2\gamma\kappa u_1 u_5)} \end{Bmatrix} \delta u_2 = \mathbf{J}_i \delta u_2 \tag{55}$$

from Eq. (54), and we have

$$\left[\frac{\partial \mathbf{H}^*}{\partial \mathbf{U}} - {}^t\Lambda\frac{\partial \mathbf{A}}{\partial \mathbf{U}}\right]\mathbf{J}_i \delta u_2 = 0 \tag{56}$$

from Eq. (49) so that for a generic increment

$$\left[\frac{\partial \mathbf{H}^*}{\partial \mathbf{U}} - {}^t\Lambda\frac{\partial \mathbf{A}}{\partial \mathbf{U}}\right]\mathbf{J}_i = 0,$$

which is a scalar relation that has to be satisfied by the components of Λ. We have four conditions for the flow problem, and one for the adjoint equations.

3.3.2. Outlet Boundary Conditions

At the outlet the situation is specular and Eq. (43) still holds. Again, the admissible variations $\delta\mathbf{U}$ must satisfy the flow boundary condition. If the regime is supersonic, the outlet conditions for the flow are determined from the interior and, conversely, the costate equations need five conditions to be prescribed at the exit. We pose $\Lambda = 0$.

If the flow is subsonic, one condition has to be supplied for $\delta\mathbf{U}$, e.g., the static pressure p at the outlet

$$p = 2\kappa e - \kappa\rho V^2 = constant. \tag{57}$$

Hence,

$$\delta p = \frac{\partial p}{\partial u_1}\delta u_1 + \frac{\partial p}{\partial u_2}\delta u_2 + \frac{\partial p}{\partial u_3}\delta u_3 + \frac{\partial p}{\partial u_4}\delta u_4 + \frac{\partial p}{\partial u_5}\delta u_5 = 0, \tag{58}$$

which gives one of the components of $\delta\mathbf{U}$, let us say δu_5, as a function of the others. As $\mathbf{n} = (0, 1, 0)$, we obtain

$$\left[\frac{\partial\mathbf{H}^*}{\partial\mathbf{U}} + {}^t\Lambda\frac{\partial\mathbf{A}}{\partial\mathbf{U}}\right]\mathbf{J}_o \begin{Bmatrix} \delta u_1 \\ \delta u_2 \\ \delta u_3 \\ \delta u_4 \end{Bmatrix} = 0, \tag{59}$$

where $\mathbf{J}$ is

$$\mathbf{J}_o = \begin{bmatrix} 1 & 0 & 0 & 0 \\ 0 & 1 & 0 & 0 \\ 0 & 0 & 1 & 0 \\ 0 & 0 & 0 & 1 \\ -\frac{V^2}{2} & u & v & w \end{bmatrix}. \tag{60}$$

Finally, from Eq. (59), we obtain

$$\left[\frac{\partial\mathbf{H}^*}{\partial\mathbf{U}} + {}^t\Lambda\frac{\partial\mathbf{A}}{\partial\mathbf{U}}\right]\mathbf{J}_o = 0, \tag{61}$$

the four boundary conditions for Λ on the outlet boundary.

3.3.3. Boundary Conditions at the Wall

At the wall we have

$$^t\Lambda\left(\frac{\partial\mathbf{A}}{\partial\mathbf{U}}n_x + \frac{\partial\mathbf{B}}{\partial\mathbf{U}}n_r\right)\delta\mathbf{U} = 0. \tag{62}$$

The no-through-flow condition at the wall requires the normal velocity component to be zero, so that the above equation becomes

$$\Lambda\{0, \delta p n_x, 0, \delta p n_r, 0\} = 0 \tag{63}$$

and finally

$$\lambda_2 n_x + \lambda_4 n_r = 0. \tag{64}$$

3.3.4. *Kinematic Adjoint Boundary Conditions*

$\delta g = 0$ at the blade leading edge, and Eq. (47) is satisfied. There is no constraint on δg at the trailing edge; hence we have

$$[\mu(\mathbf{q} \cdot \mathbf{n}) + ({}^t \Lambda \mathbf{K}) \cdot \mathbf{n}] = 0, \tag{65}$$

which is the boundary condition for the kinematic adjoint equation at the trailing edge.

3.4. Constraint on Rotor Blades

Rotor blades exchange work with the fluid. When looking for the maximum thrust, we must keep the work W, performed on the fluid per unit time, constant. The force acting on the blade is written in the form

$$F^\theta(x, r) = f(r)g(x); \tag{66}$$

therefore the work in the meridional plane per unit time is

$$W = \int_{\Omega_b} f(r)g(x)\omega r \, dr \, dx = \int_{r_h}^{r_t} f(r)\omega c(r) r \, dr, \tag{67}$$

where $c(r)$ is the chord of the blade profile and Ω_b is area of the rotor surface projected onto the meridional plane. In discrete form W can be expressed as

$$W = \sum_{i=1}^{M} f(r_i)\varphi(r_i) = \sum_{i=1}^{M} f_i \varphi_i, \tag{68}$$

where $\varphi(r_i) = \omega c(r_i) r_i (r_i - r_{i-1})$ and M is the radial number of the blade discretization points. Posing $W = W_0$, we have

$$\delta W = \sum_{i=1}^{M} \delta f_i \varphi_i = 0. \tag{69}$$

This equation is satisfied if δf and ϕ are orthogonal in the appropriate Euclidean space. The variation of Lagrangian Eq. (48) is written as

$$\delta \mathcal{L} = \int \psi \delta F^\theta \, d\Omega, \quad \psi = {}^t \Lambda \frac{\partial \mathbf{Q}}{\partial F^\vartheta}, \tag{70}$$

and in discrete form we have

$$\delta \mathcal{L} = \sum \psi_i \delta f_i. \tag{71}$$

As we are searching for the maximum thrust, we must choose the controls δf_i so that Eq. (69) is verified and the increment $\delta \mathcal{L} = \sum \psi_i \delta f_i$ assumes its highest positive value. As in the diffuser case, we obtain

$$\delta f_i = \varrho \left(\psi_i \sum_{j=1}^{M} \varphi_j^2 - \varphi_i \sum_{j=1}^{M} \psi_j \varphi_j \right). \tag{72}$$

4. ADJOINT EQUATION NUMERICAL SOLUTION

The numerical solution of the adjoint equations is obtained by using a first-order time-dependent technique based on a finite volume discretization. The solver computes the fluxes at cell interfaces using a flux-vector splitting technique. In a similar way, the boundary conditions are imposed on the numerical fluxes at the computational field edges.

Let us consider the adjoint equations. If a time derivative ${}^t\Lambda_\tau$ is added to Eqs. (42) and (43), we are led to the hyperbolic system

$$ {}^t\Lambda_\tau - {}^t\Lambda_x \mathbf{A_U} - {}^t\Lambda_r \mathbf{B_U} + {}^t\Lambda \mathbf{Q_U} + \mu \mathbf{G_U} = 0. \tag{73}$$

This system is linear, because $\mathbf{A_U}, \mathbf{B_U}, \mathbf{Q_U}$, and $\mathbf{G_U}$ only depend on x and r, and its characteristics are the same as those of the flow problem, but with opposite speeds.

In order to take advantage of a finite volume formulation which is similar to that used for the flow equations, we set

$$ {}^t\Lambda_x \mathbf{A_U} = ({}^t\Lambda \mathbf{A_U})_x - {}^t\Lambda (\mathbf{A_U})_x \tag{74}$$

$$ {}^t\Lambda_r \mathbf{B_U} = ({}^t\Lambda \mathbf{B_U})_r - {}^t\Lambda (\mathbf{B_U})_x, \tag{75}$$

and then, substituting in Eq. (73), we have

$$ {}^t\Lambda_\tau - [{}^t\Lambda \mathbf{A}_U]_x - [{}^t\Lambda \mathbf{B}_U]_r + {}^t\Lambda [(\mathbf{A}_U)_x + (\mathbf{B}_U)_r] + {}^t\Lambda \mathbf{Q_U} + \mu \mathbf{G_U} = 0. \tag{76}$$

Considering an elementary volume of integration ω with surface σ, we rewrite Eq. (76) in conservation form and apply the Gauss theorem to obtain

$$ \frac{\partial}{\partial \tau} \int_\omega {}^t\Lambda \, d\Omega - \int_\sigma {}^t\Lambda \mathbf{C} \, d\sigma + {}^t\Lambda \int_\sigma \mathbf{C} \, d\sigma + \int_\omega ({}^t\Lambda \mathbf{Q_U} + \mu \mathbf{G_U}) \, d\omega = 0, \tag{77}$$

with $\mathbf{C} = \mathbf{A_U} n_x + \mathbf{B_U} n_r$. In the previous formula we considered Λ as piecewise constant over the discretization volume. A characteristic-based approach is used to evaluate the convective fluxes at the cell interfaces. The total flux across the interface (int) is evaluated as the sum of two contributions which arise from the left (l) and right (r) sides of the interface, according to the wave-propagating nature of the hyperbolic system

$$ ({}^t\Lambda \mathbf{C})_{int} = ({}^t\Lambda^+ \mathbf{C}^+)_l + ({}^t\Lambda^- \mathbf{C}^-)_r, \tag{78}$$

where

$$ \mathbf{C}^+ = \mathbf{L} \mathbf{D}^+ \mathbf{R}, \quad \mathbf{C}^- = \mathbf{L} \mathbf{D}^- \mathbf{R}, \tag{79}$$

and $\mathbf{D}^+ + \mathbf{D}^- = \mathbf{D}$. The matrix D is

$$
\mathbf{D} = \begin{pmatrix}
V_n & 0 & 0 & 0 & 0 \\
0 & V_n & 0 & 0 & 0 \\
0 & 0 & V_n & 0 & 0 \\
0 & 0 & 0 & V_n - a & 0 \\
0 & 0 & 0 & 0 & V_n + a
\end{pmatrix}.
\tag{80}
$$

The matrices $\mathbf{D}^+$ and $\mathbf{D}^-$ are diagonal as well and they consist of the positive and negative eigenvalues of C, respectively.

The adjoint system Eq. (46) for the kinematical constraint can be manipulated in a similar way. By adding a time derivative μ_τ we have

$$
\mu_\tau - (\mu u)_x - (\mu w)_r + \nabla \cdot ({}^t\Lambda\mathbf{K}) = 0.
\tag{81}
$$

Once again the sign of the time derivate has been chosen in order to obtain a well posed problem. The finite volume approximation is straightforward;

$$
\frac{\partial}{\partial \tau} \int_{\omega_b} \mu \, d\omega - \int_{\gamma_b} \mu(un_x + wn_r) \, d\Gamma + \int_{\gamma_b} ({}^t\Lambda\mathbf{K}) \cdot \mathbf{n} \, d\Gamma = 0,
\tag{82}
$$

where ω_b is the projection of the blade surface onto the meridional plane, and γ_b its contour. The flux $\mu(un_x + wn_r)$ at the cell interfaces is taken upwind.

5. RESULTS

In the following sections we present the results for the diffuser test case and for the turbo-machinery model in the meridional plane. The grids we employ are rather coarse, as the solved flow problems do not require additional resolution. In the diffuser case we show that the results are basically unaffected by a finer grid and a larger design space.

In order to show convergence and consistency of the approach presented in the previous sections, we made sure that the gradient becomes negligible. We therefore pursued optimization steps far beyond the point where the functional has a substantial decrease: We reached O(10,000) optimization steps. For applications, only 50–100 optimization steps are acceptable. Within these limits we have reached a substantial decrease in the functional in all the illustrated cases. After the first few optimization steps, the corrections to the flow as well as to the adjoint solution also become so small that only a few relaxation steps in the respective solvers are needed for convergence. The most expensive case presented, the two counterrotating rotors, requires about 20 h of CPU time on a Digital Alpha 600 Workstation after 10,000 optimization steps.

5.1. Diffuser

The diffuser is discretized over a 40×20 grid. The inlet pressure is $p_{in} = 0.83$, the outlet pressure $p_{out} = 0.944$. The imposed flow angle at the inlet varies from zero, at the bottom wall, to 10 degrees, at the upper wall. We are looking for the diffuser geometry that best approximates a zero flow angle at the outlet. As explained, the control is represented here by the pressure gradient at each computational point lying on the upper wall. The number of design variables is one less than the grid discretization in the x-direction. If a usual shape

optimization method were to be applied in this case, we would obtain an additional adjoint partial differential equation. The initial wall pressure distribution is a parabolic profile (see Fig. 6) that satisfies the constraint on the pressure gradient in Fig. 1.

The initial and final geometry of the diffuser are depicted in Fig. 3. The initial geometry is characterized by a nonzero flow angle $\sigma(y)_{out}$ at the exit. The l^2 norm of the gradient
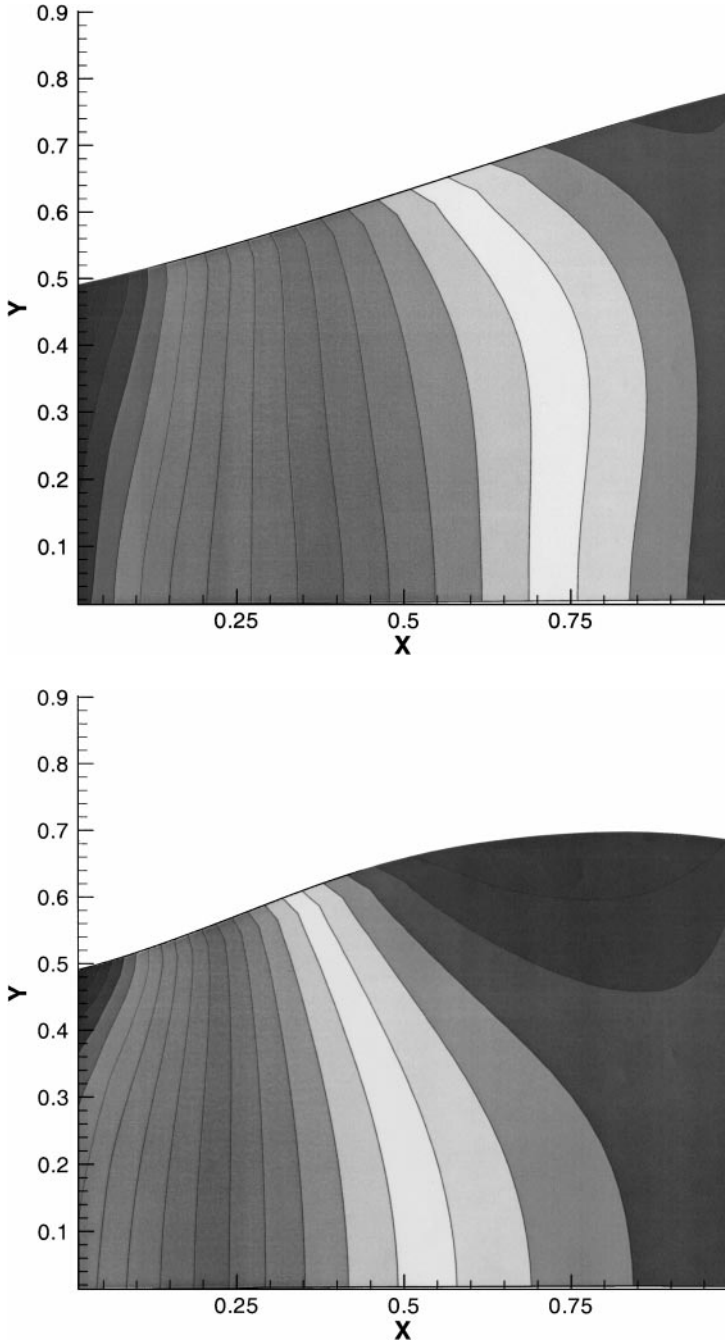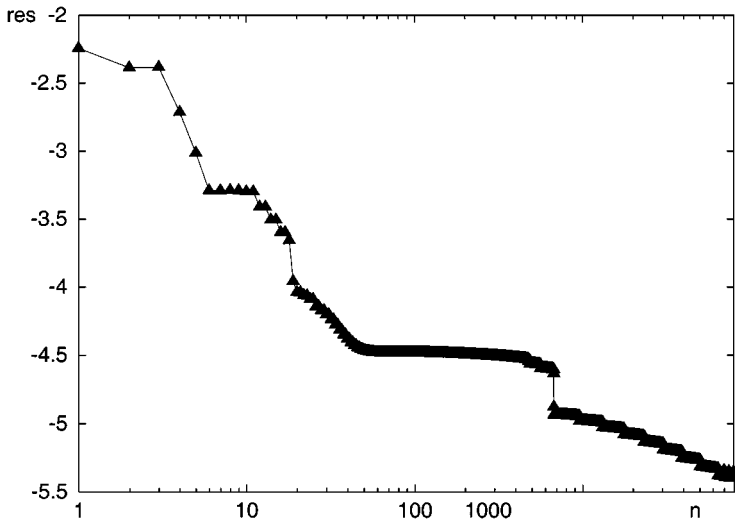

FIG. 3. Diffuser. The geometry and pressure field before (Top) and after (Bottom) the optimization process.
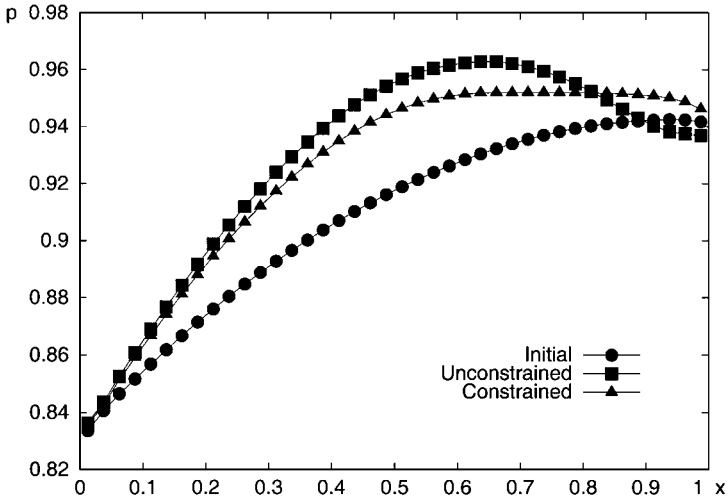
FIG. 4. Diffuser. Gradient residual *res* versus optimization step n.

residuals is presented in Fig. 4. The functional D decreases noticeably (see Fig. 5), but because of the pressure gradient constraint, the flow is not perfectly axial at the outlet.

The pressures displayed in Fig. 6 are relative to the cell centers next to the diffuser wall. The initial and optimal configurations are shown. The unconstrained optimal wall pressure distribution is depicted in the same figure. The small outlet pressure differences are due to the various geometries pertinent to each case.

The used mesh makes the problem computationally quite small. Indeed, in such a simple problem there are 40 design variables with strictly enforced inequality constraints on the pressure gradient. We have increased the spatial resolution to 80×40 grid points, thus using 80 design variables. Even when the design space is doubled, the results obtained, in terms of the pressure distribution, do not remarkably change, as seen in Fig. 7.

FIG. 5. Diffuser. Flow alignment D versus optimization step n.

FIG. 6. Diffuser. Optimal pressure distribution on the upper wall, initial pressure distribution, and unconstrained optimal distribution.

5.2. Fan Stage

The distributed control F^θ is null everywhere except on the blades and is

$$F^\theta(x, x_i) = \mathcal{F}(r_i)\left[1 - \cos\left(2\pi \frac{x - x_t}{x_l - x_t}\right)\right] \tag{83}$$

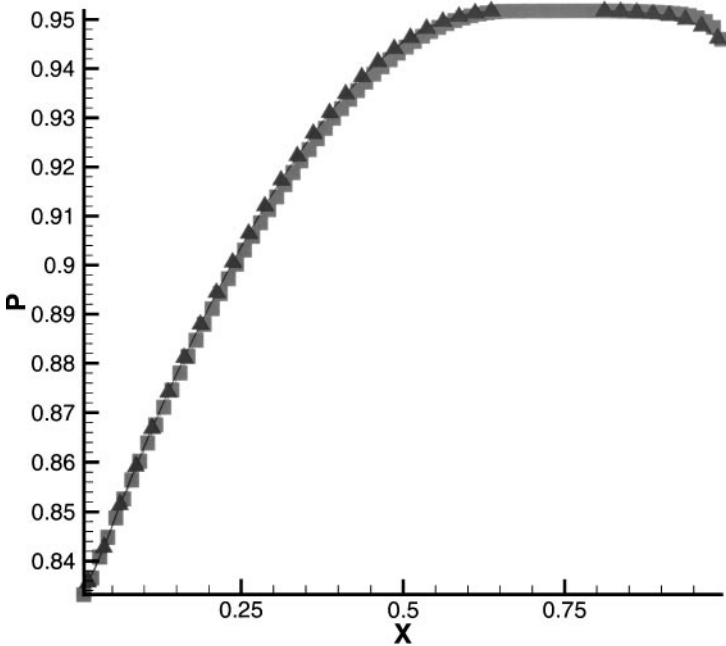so that the load on the leading ($x = x_l$) and trailing ($x = x_t$) edges is 0. For each considered

FIG. 7. Diffuser. Optimal pressure distribution with constraints on the allowed gradient. Results for a 40×20 mesh versus those obtained with an 80×40 mesh.
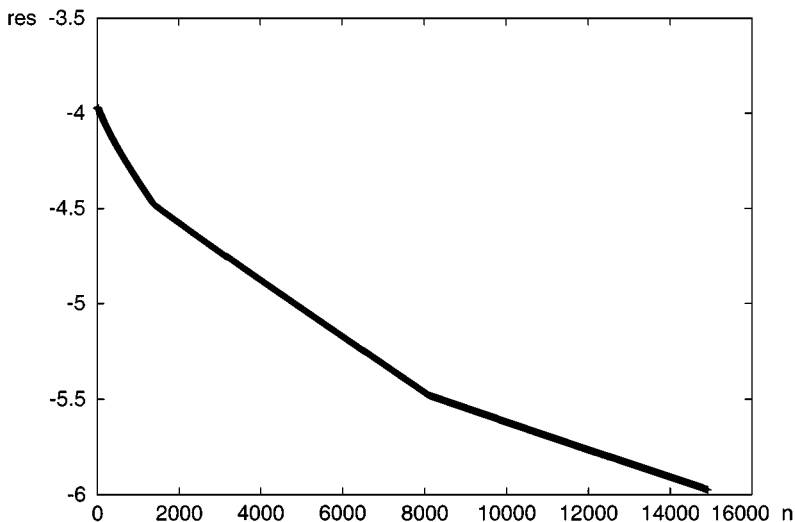
FIG. 8.   Fan stage. Gradient residual versus optimization steps.

blade, we have as many design parameters $\mathcal{F}(r_i)$ as the number of computational points in the radial direction.

Therefore, Eq. (48) is discretized as

$$\delta\mathcal{L} = \sum_i \delta\mathcal{F}(r_i)L(r_i)(r_i - r_{i-1}), \tag{84}$$

where

$$L(r_i) = \sum_j {}^t\Lambda(r_i, x_j)\frac{\partial \mathbf{Q}}{\partial F^\vartheta}(r_i, x_j)\left[1 - \cos\left(2\pi\frac{x_j - x_t}{x_l - x_t}\right)\right](x_j - x_{j-1}).$$

The design variables for this test case, where the grid is 60×24, are 24 for the stator and
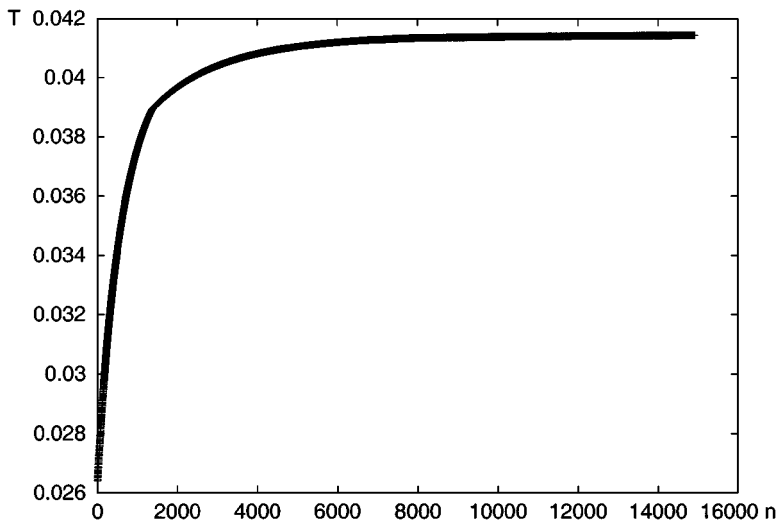
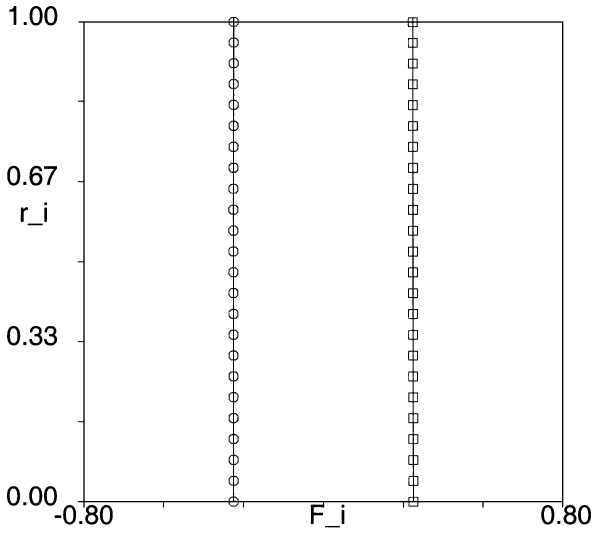**FIG. 9.**   Fan stage. Thrust versus optimization steps.

FIG. 10. Counterrotating rotors. Initial force distribution $\mathcal{F}_i$ on the blade.

24 for the rotor; $\omega = 1.58$ and on the rotor the work is fixed to that relative to the initial force distribution. The constraint on the total work performed by the rotor allows very small variations of the force distribution on the rotor itself. This is seen in the gradient components relative to the rotor which are two orders of magnitude smaller than those relative to the stator. In a different test case relative to a single rotor but not shown here, we found that for a gradient residual decrease of two orders of magnitude, the thrust gain is very limited.

In the initial configuration, the stator does not exert any force on the flow, that is, it coincides with a force-free stream surface. The gradient residual in Fig. 8 and the thrust in Fig. 9 are plotted against the optimization step. After the computation of the first flow and
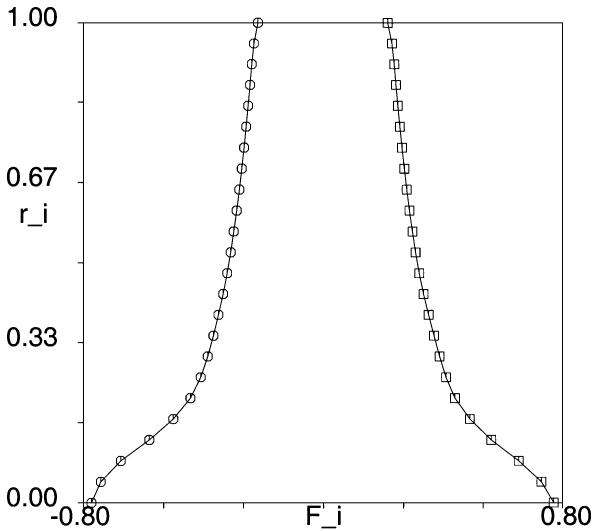
FIG. 11. Final force distribution.

adjoint fields, each optimization step takes a significantly reduced amount of computational time. The gradient decreases by more than two orders of magnitude and the thrust increases by about 100%.

We consider an additional test case belonging to the same class of problem; two coun-terrotating ducted fans. The counterrotating fan case is discretized on a 75×25 grid, with
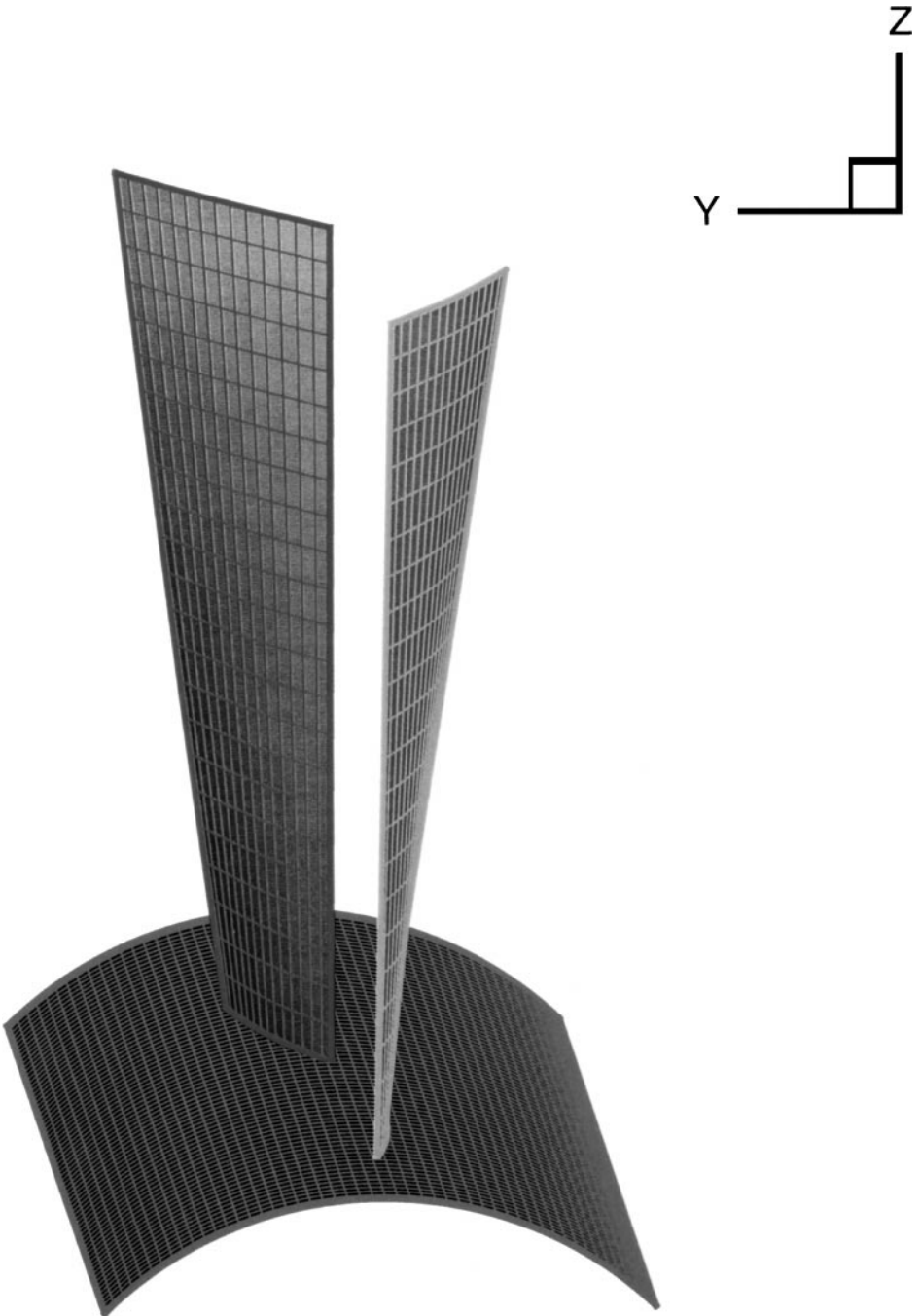

FIG. 12. Counterrotating rotors. Initial geometry.

24×2 design variables. Again the total work performed by the rotors is fixed and equal to that of the initial force configuration. The two rotation speeds are $\omega_1 = -\omega_2 = 0.4$. The initial force radial distribution is constant on both blades. The thrust increases from 0.0235 to 0.0285 and reaches its asymptotic value after 20 design cycles. The computation was pursued until the gradient was reduced by three orders of magnitude. The solution of the maximum thrust is one with minimal axial deviation at the exit, and a force radial distribution quite far from the initial guess. We show the initial and final force configurations in Figs. 10 and 11. The solution in terms of force distribution is symmetric as expected. The initial and final geometries of the blades are presented in Figs. 12 and 13.
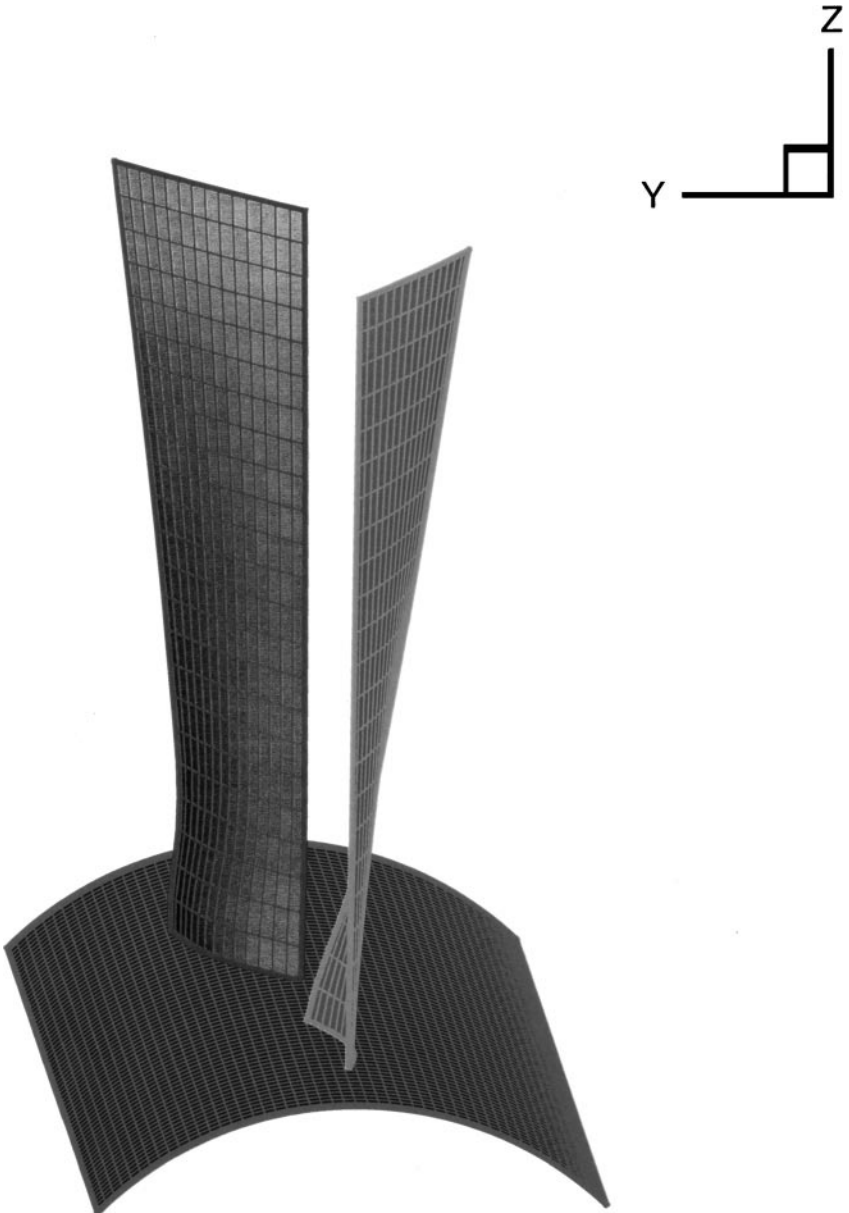

FIG. 13.   Counterrotating rotors. Final geometry.

6. CONCLUSIONS

In this work we derive an adjoint optimization method for aerodynamic design based on the solution of the inverse problem. We apply it to diffuser and turbo-machinery design. It takes advantage of the inverse solution of the flow equations to determine optimal configurations. The flow constraints are imposed directly into the parameterization of the flow distribution that has to be optimized. No additional Lagrange multipliers are needed to satisfy such constraints. The relative advantages of using this approach compared to the usual shape design optimization should be evaluated case by case considering the number of flow constraints versus the number of geometric constraints. We believe this approach to be more efficient for aerodynamic components where the flow quality is crucial.

APPENDIX

$$
\mathbf{A}_U =
\begin{bmatrix}
0 & 1 & 0 & 0 & 0 \\
\kappa V^2 - u^2 & -2(\kappa - 1)u & -2\kappa v & -2\kappa w & 2\kappa \\
-uv & v & u & 0 & 0 \\
-uw & w & 0 & u & 0 \\
u\left(2\kappa V^2 - \frac{\gamma e}{\rho}\right) & \frac{\gamma e}{\rho} - \kappa(V^2 + 2u^2) & -2\kappa uv & -2\kappa uw & \gamma u
\end{bmatrix}
\tag{85}
$$

$$
\mathbf{B}_U =
\begin{bmatrix}
0 & 0 & 0 & 1 & 0 \\
-uw & w & 0 & u & 0 \\
-vw & 0 & w & v & 0 \\
\kappa V^2 - w^2 & -2\kappa u & -2\kappa v & -2(\kappa - 1)w & 2\kappa \\
w\left(2\kappa V^2 - \frac{\gamma e}{\rho}\right) & -2\kappa uw & -2\kappa vw & \frac{\gamma e}{\rho} - \kappa(V^2 + 2w^2) & \gamma w
\end{bmatrix}
\tag{86}
$$

$$
\mathbf{Q}_U =
\begin{bmatrix}
0 & \alpha & 0 & \frac{1}{r} & 0 \\
-\frac{uw}{r} - \frac{u\alpha}{\rho} & \frac{w}{r} + 2u\alpha & 0 & \frac{u}{r} & 0 \\
-\frac{2vw}{r} & 0 & \frac{2w}{r} & \frac{2v}{r} & 0 \\
\frac{w^2 - v^2}{r} & 0 & \frac{2v}{r} & -\frac{2w}{r} & 0 \\
q_{51} & q_{52} & q_{53} & q_{54} & \gamma\frac{w}{r} + u\alpha
\end{bmatrix}
\tag{87}
$$

$$
q_{51} = -\frac{F^\theta}{\rho}(urg_x + wrg_r - v) - \left(\frac{\gamma e}{\rho} - 2\kappa V^2\right)\left(\frac{w}{r} + u\alpha\right)
\tag{88}
$$

$$
q_{52} = \frac{F^\theta}{\rho}rg_x + \alpha\left(\frac{\gamma e}{\rho} - \kappa V^2\right) - 2\kappa\left(\frac{w}{r} + u\alpha\right)
\tag{89}
$$

$$
q_{53} = -\frac{F^\theta}{\rho} + 2\kappa v\left(\frac{w}{r} + u\alpha\right)
\tag{90}
$$

$$
q_{54} = \frac{F^\theta}{\rho}rg_r + \frac{1}{r}\left(\frac{\gamma e}{\rho} - 2\kappa V^2\right) - 2\kappa w\left(\frac{w}{r} + u\alpha\right)
\tag{91}
$$

$$
\frac{\partial \mathbf{Q}}{\partial F^\theta} = \{0, \, rg_x, \, -1, \, rg_r, \, rg_xu + rg_rw - v\}
\tag{92}
$$

$$\frac{\partial H}{\partial U} = \{0, \ g_x, \ -\frac{1}{r}, \ g_r, \ 0\} \tag{93}$$

$$\frac{\partial H^*}{\partial \mathbf{U}} = \{\kappa V^2 - u^2, \ -2(\kappa - 1)u, \ -2\kappa v, \ -2\kappa w, \ 2\kappa\} \tag{94}$$

$$
\mathbf{L} =
\begin{bmatrix}
1 - \frac{\kappa V^2}{a^2} & \frac{2\kappa u}{a^2} & \frac{2\kappa v}{a^2} & \frac{2\kappa w}{a^2} & \frac{2\kappa}{a^2} \\
\frac{V_t}{\rho} & \frac{n_r}{\rho} & 0 & \frac{n_x}{\rho} & 0 \\
-\frac{v}{\rho} & 0 & -\frac{1}{\rho} & 0 & 0 \\
\frac{\kappa V^2 - aV_n}{2a^2} & \frac{an_x - 2\kappa u}{2a^2} & -\frac{\kappa v}{a^2} & \frac{an_r - 2\kappa w}{2a^2} & \frac{\kappa}{a^2} \\
\frac{aV_n + 2\kappa V^2}{2a^2} & -\frac{an_x + 2\kappa u}{2a^2} & -\frac{\kappa v}{a^2} & -\frac{an_r + 2\kappa w}{2a^2} & \frac{\kappa}{a^2}
\end{bmatrix}
\tag{95}
$$

$$
\mathbf{R} =
\begin{bmatrix}
1 & 0 & 0 & 1 & 1 \\
u & \rho n_r & 0 & u + an_x & u - an_x \\
v & 0 & \rho & v & v \\
w & -\rho n_x & 0 & w + an_r & w - an_r \\
\frac{V^2}{2} & \rho V_t & \rho v & \frac{a^2 + \kappa V^2}{2k} + aV_n & \frac{a^2 + \kappa V^2}{2k} - aV_n
\end{bmatrix}.
\tag{96}
$$

REFERENCES

1. W. Mangler, Die berechnung eines tragflugelprofiles mit vorgeschriebener druckverteilung, *Jahrb. Deutsch. Luftfahrtforschung* **1**, 46 (1938).

2. J. M. Lighthill, *A New Method of Two-Dimensional Aerodynamic Design*, Aeronautics Research Council Reports and Memoranda 2112 (1945).

3. A. M. Elizarov, N. B. Il'inskiy, and A. V. Potashev, *Mathematical Methods of Airfoil Design* (Akademie Verlag, Berlin, 1997).

4. L. Polito, *Un Metodo Esatto per il Progetto di Profili Alari in Corrente Incompressibile Aventi un Prestabilito Andamento della Velocià sul Contorno*, Università di Pisa, Rapporto Istituto di Aeronautica 42 (1974).

5. F. Bauer, P. Garabedian, and D. Korn, *Supercritical Wing Sections* (Springer-Verlag, Berlin/New York, 1972).

6. G. Volpe, *Geometric and Surface Pressure Restrictions in Airfoil Design*, AGARD-R-780 (1990).

7. O. Pironneau, On optimum design in fluid mechanics, *J. Fluid Mech.* **59**, 117 (1972).

8. A. Jameson, *Aerodynamic Design via Control Theory*, ICASE Report, 88–64; *J. Sci. Comput.* **3**, 233 (1988).

9. A. Jameson, Optimum aerodynamic design using control theory, in *Computational Fluid Dynamics Review*, edited by M. Hafez (John Wiley & Sons, 1995) p. 495.

10. A. Jameson, L. Martinelli, and N. A. Pierce, Optimum aerodynamic design using the Navier–Stokes equations, *Theoret. Comput. Fluid Dynam.* **10**, 213 (1998).

11. R. F. van den Dam, J. A. van Egmond, and J. W. Sloof, *Optimization of Target Pressure Distributions*, AGARD-R-780 (1990).

12. J. Elliot and J. Peraire Constrained, multipoint shape optimization for complex 3D configurations, *Aeronaut. J.* **Aug./Sept.** 365 (1998).

13. C. Bena, F. Larocca, and L. Zannetti, Design of multistage axial flow turbines and compressors, in *IMech-E 3rd European Conference on Turbomachinery Proceedings, London, 1999* (Professional Engineering Publishers, London, 1999) p. 635.

14. B. S. Stratford, The prediction of separation of the turbulent boundary layer, *J. Fluid Mech.* **5**, 1 (1954).

15. L. Zannetti, A time-dependent method to solve the inverse problem for internal flows, *AIAA J.* **18**, 754 (1980).

16. L. Zannetti and F. Larocca, *Inverse Methods for 3D Internal Flows*, AGARD-R-780 (1990).

17. M. Pandolfi, A contribution to the numerical prediction of unsteady flows, *AIAA J.* **22**, 602 (1984).

18. A. Harten, B. Engquist, and S. Osher, Uniformly High-order-accurate essentially nonoscillatory schemes, III, *J. Comput. Phys.* **71**, 231 (1987).

19. F. Beux and A. Dervieux, Exact-gradient shape optimization of a 2-D Euler flow, *Finite Elem. Anal. Design* **12**, 281 (1992).

20. A. Iollo and M. D. Salas, Contribution to the optimal shape design of 2D internal flows with embedded shocks, *J. Comput. Phys.* **125**, 124 (1996).

21. R. Fletcher, *Practical Methods of Optimization* (Wiley, New York, 1980).